Two-dimensional P1 approximation (P1-2D) for the Description of the Radiant Field on Cylindrical Solar Photocatalytic Reactors

Clovis Nchikou

INTERLINE Institute of Higher Studies. Faculty of Chemical, Mechanical, and Electrical Engineering. 20 de noviembre 316 Sur, Centro, 67485 Cadereyta Jiménez, Nuevo León, México.

ABSTRACT

The local volumetric rate of photon absorption (*LVRPA*) was formulated by solving the radiative transfer equation (RTE) in polar coordinates with the P1 approximation approach (P1-2D) for the description of the radiant field in cylindrical solar photocatalytic reactors. A general expression of the *LVRPA* was formulated that can be employed on cylindrical photocatalytic reactors with an incident radiation constant along the reactor length. CPC and tubular photocatalytic reactors were used as reactor models and Lambert's cosine law (irradiance) was considered when using the boundary conditions. Simulations were carried out using the commercial TiO2-P25, its optical properties taken from the literature. The *LVRPA* was found to decrease exponentially from the reactor wall to its center. literature rate of photon absorption per unit of reactor length (*VRPA/H*) increased exponentially with the catalyst loading until a value where no significant increase was observed and was found to increase with reactor radius, information that agrees with the literature. The optimum catalyst loading with the CPC reactor was about 0.364 g/L with a reactor radius equal to 1.65 cm similar to that found in the literature when using the six-flux model in two dimensions (SFM-2D). The apparent optical thickness τ_{App1} newly formulated with the P1 approximation was introduced for optimization purposes and was found more reliable than the optical thickness τ. This parameter not only removes the dependence of the optimum catalyst loading on the reactor's radius but also its dependence on catalyst albedo. τ_{App1} was found about 9.73 and 14.6 for CPC and tubular reactors respectively and provides the optimum catalyst loading and the reactor radius that optimize the radiation absorption inside both reactors.

Keywords: Six-flux model; LVRPA; photoreactor.

Aproximación bidimensional P1 (P1-2D) para la descripción del campo radiante en reactores solares fotocatalíticos cilíndricos

RESUMEN

Se formuló la velocidad volumétrica local de absorción de fotones (LVRPA) resolviendo la Ecuación de Transferencia Radiativa (RTE) en coordenadas polares con la aproximación P1 (P1-2D) para la descripción del campo radiante en reactores solares fotocatalíticos cilíndricos. Se formuló una expresión general del LVRPA que puede emplearse en reactores fotocatalíticos cilíndricos con una radiación incidente constante a lo largo de la longitud del reactor. Se utilizaron reactores fotocatalíticos CPC y tabulares como modelos de reactor y se consideró la ley del coseno de

Lambert (irradiancia) al utilizar las condiciones de contorno. Las simulaciones se realizaron utilizando el TiO2-P25 comercial cuyas propiedades ópticas se tomaron de la bibliografía. Se encontró que el LVRPA disminuye exponencialmente desde la pared del reactor hacia su centro. La velocidad volumétrica de absorción de fotones por unidad de longitud del reactor (VRPA/H) aumentó exponencialmente con la carga de catalizador hasta un valor en el que no se observó un aumento significativo y se encontró que aumentaba con el radio del reactor, información que concuerda con la literatura. La carga óptima de catalizador con el reactor CPC fue de aproximadamente 0,364 g/L con un radio del reactor igual a 1,65 cm, similar a la encontrada en la literatura cuando se utilizó el modelo de seis flujos en dos dimensiones (SFM-2D). El espesor óptico aparente $\tau_{\_App1}$ formulado de nuevo con la aproximación P1 se introdujo con fines de optimización y se encontró más fiable que el espesor óptico τ. Este parámetro no sólo elimina la dependencia de la carga óptima de catalizador del radio del reactor, sino también su dependencia del albedo del catalizador. El $\tau_{\_App1}$ se encontró alrededor de 9,73 y 14,6 para CPC y reactores tubulares, respectivamente, y proporciona la carga óptima de catalizador y el radio del reactor que optimizan la absorción de radiación dentro de ambos reactores.

Palabras clave: Six Flux Model; LVRPA; Fotorreactor.

1. Introduction

Water contamination is a serious global concern, particularly impacting underdeveloped countries. Several ways have been proposed to overcome this issue. For many decades, heterogeneous photocatalysis has been regarded as a viable oxidation approach for disinfecting and decontaminating water [1], [2]. It is an advanced oxidation technology that uses solar or artificial radiation to photoexcite photocatalysts. When a semiconductor is activated with energy equal to or higher than its band gap energy, electron-hole pairs form. When these pairs come into contact with charge carriers (H2O, OH−, O2, etc.), they produce radical oxidative species such as hydroxyl radicals. These radicals are transitory molecules that target pollutants found in the fluid phase via oxidative or reductive reaction pathways [3]. Research on solar photocatalysis as a clean technology for producing hydrogen and solar fuels, as well as a sustainable alternative to treating industrial wastewater and removing organic pollutants, dyes, pesticides, and emerging contaminants, has increased significantly as a result of the ongoing concern about water remediation [4], [5]. Mathematical modeling has become increasingly relevant in this field since it has been used as a powerful and vital tool for the design of photoreactors of different configurations [6]. The mathematical modeling of photocatalysis processes is built on a series of sub-models, including the modeling of the radiant field [7]. This sub-model is composed of the solar emission and the absorption-scattering models for the evaluation of the LVRPA, one of the main parameters of the intrinsic kinetic equation [8]. The LVRPA strongly depends on the reactor configuration, radiation source, catalyst load, and type of photocatalyst, in some cases on the contaminant when this absorbs the radiant energy. For its formulation, the RTE should be solved, with its integro-differential form [9] which makes this task very challenging to accomplish. Eq. (1) shows the steady-state and non-temperature-dependence of the RTE, which describes the different phenomena that occur on the light when it traverses a medium, such as absorption, in-scattering, and out-scattering as represented in Eq. (1).

$$\frac{dI_\lambda(S,\Omega)}{ds} = -KI_\lambda(S,\Omega) - \sigma_\lambda I_\lambda(S,\Omega) + \frac{\sigma_\lambda}{4\pi}\int_{\Omega=4\pi} P(\Omega' \to \Omega)I_\lambda(S,\Omega')d\Omega' \tag{1}$$

where I_λ is the photon irradiance (W/m^2), K_λ the absorption coefficient (m^2/kg), σ_λ the scattering coefficient (m^2/kg), $P(\Omega' \to \Omega)$ the scattering phase function, λ the wavelength (m), S the spatial coordinate (m) and Ω the directional solid angle (Steradian) [10-12].

Several numerical techniques, such as the discrete ordinate methods (DOM) and the Monte Carlo model, were employed to solve the RTE; However, these techniques are time-consuming and require large processing resources [13-15]. Alternative analytic methods such as the n-flux or the Pn approximation models (n is a strictly positive integer) have been implemented to solve the RTE and have been satisfactorily used for the description and estimation of the radiant field in various types of photocatalytic reactors [16], [17]. As the name suggests, the P1-approximation is the simplest form of the spherical harmonics method. It only uses the first two terms of the Pn approximation [18-20]. It is more versatile than two and four-flux models because it lends itself more easily to different geometries [16]. It has been used to solve the RTE in one dimension in flat plate photoreactors and two dimensions in parabolic photoreactors [16], [21]. The P1 approximation saves computational time and effort by reducing the mathematical complexity of the RTE to an analytical equation [16], [17], [21]. CPC photocatalytic reactors are cylindrical reactors with the ability to receive radiation not only on their side exposed to the sun but also on their side hidden from it. They can be scaled up and can be used with solar radiation, so they are very attractive and provide an excellent configuration for efficient activation of the photocatalyst TiO_2 [22], [23]. Their modeling requires a complex analysis of the radiation field inside the photoreactor [24-26].

In this study, an analytic expression of the LVRPA for cylindrical solar photocatalytic reactors with incident radiation constant along the reactor length was derived and special cases of tubular and CPC were addressed. Lambert's cosine law (irradiance) was considered in the boundary conditions when running the simulations. Lambert's cosine law stipulates that the incoming radiation at a point on a surface is proportional to the cosine of the incidence angle between the normal vector and the incident beam that hits the point; The fluence rate, unlike the irradiance considers the entire radiation intensity reaching the boundary [15], [25], [27]. A new dimensionless optimization parameter, the apparent optical thickness (τ_{App1}) was introduced with the P1 approximation approach, this parameter was recently applied to flat plate photocatalytic reactors [28]. The commercial titanium dioxide Degussa P-25 was used as a catalyst model with its optical properties taken from the literature [24].

2. Methodology

2. 1 Mathematical modeling for the radiant field

The radiant field was estimated by solving the RTE in two dimensions (in polar coordinates), and then the $LVRPA$ was deduced. Eq. (2) is the governing equation of the P1 approximation or the so-called Helmholtz's equation which will be solved later with suitable boundary conditions.

$$\Delta G_\lambda = \frac{1}{r}\frac{\partial\left(r\frac{\partial G_\lambda}{\partial r}\right)}{\partial r} + \frac{1}{r^2}\frac{\partial^2 G_\lambda}{\partial\theta^2} + \frac{\partial G_\lambda}{\partial z} = k_{d,\lambda}^2 G_\lambda \tag{2}$$

where,

$$k_{d,\lambda} = \beta_\lambda\sqrt{3(1-\omega_\lambda)\left(1-g_\lambda\frac{\omega_\lambda}{3}\right)} \tag{3}$$

where g_λ is the asymmetry factor corresponding to the monochromatic radiation of wavelength λ and which is proper to each catalyst, β_λ is the monochromatic extinction coefficient being the sum of κ_λ and σ_λ which are the monochromatic absorption and scattering coefficients respectively defined as,

$$\beta_\lambda = \kappa_\lambda + \sigma_\lambda \tag{4}$$

All of these coefficients linearly depend on catalyst particle concentration, as,

$$\beta_\lambda = \beta_\lambda^\star C_{cat}, \kappa_\lambda = \kappa_\lambda^\star C_{cat}, \ \sigma_\lambda = \sigma_\lambda^\star C_{cat} \tag{5}$$

where C_{cat} is the catalyst concentration, $\beta_\lambda^\star$, $\kappa_\lambda^\star$ and $\sigma_\lambda^\star$ are specific coefficients, independent of this concentration (for values in the usual ranges for photocatalysis).

ω_λ is the scattering albedo which gives the probability that a photon is scattered when colliding with a particle defined as,

$$\omega_\lambda = \frac{\sigma_\lambda}{\beta_\lambda} \tag{6}$$

Instead of using the monochromatic parameters, one should use their average values in a defined wavelength interval $[\lambda_{min}, \lambda_{max}]$ using the following equation,

$$\Gamma^* = \frac{\int_{\lambda_{min}}^{\lambda_{max}} \Gamma_\lambda I(\lambda) d\lambda}{\int_{\lambda_{min}}^{\lambda_{max}} I(\lambda) d\lambda} \tag{7}$$

where Γ_λ can be one of the parameters κ_λ , $\sigma_\lambda, \beta_\lambda$ or g_λ and λ_{min}=280 nm, λ_{max}=395 nm given by the interception of solar emission spectrum and titanium dioxide absorption spectrum; $I(\lambda)$ is the spectrum of solar emission power [29].

G_λ is the local radiation which corresponds to the integration of the irradiance I_λ all over the solid angle Ω. After finding the expression of G_λ, one can easily deduce the local volumetric rate of photon absorption ($LVRPA$) from Eq. (8); this parameter is very important for the determination of the intrinsic kinetic rate equation of any photocatalytic reaction system.

$$LVRPA = (k_\lambda + \kappa_c)G_\lambda \tag{8}$$

where k_λ and κ_c are the catalyst and contaminant absorption coefficients respectively.
The volumetric rate of photons absorption per unit reactor length, $VRPA/H$ which describes the distribution of the photon absorption inside the reactor gives a broader view of the energy absorption since it does not depend on the reactor length. It is defined later in this work and obtained by integrating the $LVRPA$ over the circular cross section of the reactor. The overall volumetric rate of photons absorption (OVRPA) is obtained just by multiplying the $VRPA/H$ by the reactor length.

Eq. (2) in polar coordinates results in,

$$r\frac{\partial^2 G_\lambda}{\partial r^2} + \frac{\partial G_\lambda}{\partial r} + \frac{1}{r}\frac{\partial^2 G_\lambda}{\partial \theta^2} - k_{d,\lambda}^2 r G_\lambda = 0 \tag{9}$$

Eq. (11) is solved using the method of separation of variables, by assuming $G_\lambda = G_{r,\lambda}G_{\theta,\lambda}$ where $G_{r,\lambda}$ and $G_{\theta,\lambda}$ are functions of r and θ respectively.

Dividing Eq. (9) by $G_{r,\lambda}G_{\theta,\lambda}$ and rearranging, one finds,

$$\frac{r\left(r\frac{\partial^2 G_{r,\lambda}}{\partial r^2} + \frac{\partial G_{r,\lambda}}{\partial r}\right)}{G_{r,\lambda}} - k_{d,\lambda}^2 r^2 = -\frac{\frac{\partial^2 G_{\theta,\lambda}}{\partial \theta^2}}{G_{\theta,\lambda}} \tag{10}$$

The terms at the left and right-hand sides of Eq. (10) depend exclusively on r and θ respectively but since they are equal, they should be a real constant η. Then, Eq. (10) results in Eqs. (11-12)

$$r^2\frac{\partial^2 G_{r,\lambda}}{\partial r^2} + r\frac{\partial G_{r,\lambda}}{\partial r} - \left(k_{d,\lambda}^2 r^2 + \eta\right)G_{r,\lambda} = 0 \tag{11}$$

$$\frac{\partial^2 G_{\theta,\lambda}}{\partial \theta^2} = -\eta G_{\theta,\lambda} \tag{12}$$

By changing the variable r by $r_1 = k_{d,\lambda}r$, Eq. (11) turns to

$$r_1^2\frac{\partial^2 G_{r_1,\lambda}}{\partial r_1^2} + r_1\frac{\partial G_{r_1,\lambda}}{\partial r_1} - \left(r_1^2 + \eta\right)G_{r_1,\lambda} = 0 \tag{13}$$

Assuming η positive, Eq. (13) is the modified Bessel differential equation which has the general solution,

$$G_{r_1,\lambda}(r_1) = G_{r,\lambda}(r) = A_\eta I_\eta(k_{d,\lambda}r) + B_\eta K_\eta(k_{d,\lambda}r) \tag{14}$$

where I_η are K_η modified Bessel functions of first and second kind respectively.

The general solution for Eq. (14) is:

$$G_{\theta,\lambda} = C_\eta \cos(\sqrt{\eta}\theta) + D_\eta \sin(\sqrt{\eta}\theta) \tag{15}$$

where A_η, B_η, C_η, and D_η are real constants.

Considering that physically the specific intensity of the radiation G_λ must be 2π−periodic with respect to θ (Arancibia-Bulnes et al., 2009; Nchikou et al., 2021), then $G_{\theta,\lambda}$ should be also 2π−periodic with respect to θ and $\sqrt{\eta}$ should take the values $n = 0,1,2, ...$, then $\eta = n^2$, $n = 0,1,2, ...$

Finally, the general solution of Eq. (9) is the superposition of the set of solutions (one must consider all eigenfunctions). Then, the general solution for Eq. (9) is,

$$G_\lambda = \sum_{n=0}^{+\infty}\left(A_n I_n(k_{d,\lambda}r) + B_n K_n(k_{d,\lambda}r)\right)(C_n\cos(n\theta) + D_n \sin(n\theta)) \tag{16}$$

G_λ is a Fourier series in terms of angular coordinate, thus, for the determination of the integration constants, it is necessary to expand the incident radiation reaching the reactor wall G_0 as a Fourier series [16], [25] as follows,

$$G_0 = \frac{h_0}{2} + \sum_{n=1}^{+\infty}[h_n cos(n\theta) + w_n sin(n\theta)] \tag{17}$$

where h_n and w_n are G_0 Fourier series expansion constants defined by Eqs. (18-20) using the so-called orthogonality relations between sine and cosine functions.

$$h_0 = \frac{1}{\pi}\int_0^{2\pi} G_0 d\theta \tag{18}$$

$$h_n = \frac{1}{\pi}\int_0^{2\pi} G_0 cos(n\theta) d\theta \tag{19}$$

$$w_n = \frac{1}{\pi}\int_0^{2\pi} G_0 sin(n\theta) d\theta \tag{20}$$

For cylindrical reactors receiving radiation from their external wall, one should make sure that the radiation intensity does not diverge at the reactor center ($r = 0$).
In this case, since K_n diverges when $r = 0$, B_n should be taken zero. Then, Eq. (16) leads to,

$$G_\lambda = \sum_{n=0}^{+\infty} A_n I_n(k_{d,\lambda}r)(C_n cos(n\theta) + D_n sin(n\theta)) \tag{21}$$

The integration constant A_n should be determined using the Marshak's boundary condition [30] with respect the radial coordinate as follows,

$$G_\lambda(R,\theta) + \frac{2}{3\xi_\lambda}\frac{dG_\lambda}{dr}\bigg|_{r=R} = 4G_0(R,\theta) \tag{22}$$

which implies,

$$\sum_{n=0}^{+\infty} A_n\left(I_n(k_{d,\lambda}R) + \frac{2}{3\xi_\lambda}I_{n+1}(k_{d,\lambda}R)\right)(C_n cos(n\theta) + D_n sin(n\theta)) = 4G_0 \tag{23}$$

For $n = 0$, $D_0 = 0$ and, $C_0 = \frac{1}{2\pi}\int_0^{2\pi} G_0 d\theta$,

$$A_0 = \frac{4}{I_0(k_{d,\lambda}R) + \frac{2}{3\xi_\lambda}I_1(k_{d,\lambda}R)} \tag{24}$$

For $n > 0$,

$$A_n C_n\left(I_n(k_{d,\lambda}R) + \frac{2}{3\xi_\lambda}I_{n+1}(k_\lambda R)\right) = \frac{4}{\pi}\int_0^{2\pi} G_0 cos(n\theta) d\theta \tag{25}$$

$$A_n D_n \left(I_n(k_{d,\lambda} R) + \frac{2}{3\xi_\lambda} I_{n+1}(k_\lambda R) \right) = \frac{4}{\pi} \int_0^{2\pi} G_0 \sin(n\theta) d\theta \tag{26}$$

$$\frac{C_n}{D_n} = \frac{\frac{1}{\pi} \int_0^{2\pi} G_0 \cos(n\theta) d\theta}{\frac{1}{\pi} \int_0^{2\pi} G_0 \sin(n\theta) d\theta} \tag{27}$$

By taken $C_n = \frac{1}{\pi} \int_0^{2\pi} G_0 \cos(n\theta) d\theta$ and $D_n = \frac{1}{\pi} \int_0^{2\pi} G_0 \sin(n\theta) d\theta$,

$$A_n = \frac{4}{I_n(k_{d,\lambda} R) + \frac{2}{3\xi_\lambda} I_{n+1}(k_{d,\lambda} R)} \tag{28}$$

Combining Eqs. (21, 28) results in the specific intensity of the radiation as follows:

$$G_\lambda = \frac{4 I_0(k_{d,\lambda} r) \left(\frac{1}{2\pi} \int_0^{2\pi} G_0 d\theta \right)}{I_0(k_{d,\lambda} R) + \frac{2}{3\xi_\lambda} I_1(k_{d,\lambda} R)} +$$

$$\sum_{n=1}^{+\infty} \frac{4 I_n(k_{d,\lambda} r)}{I_n(k_{d,\lambda} R) + \frac{2}{3\xi_\lambda} I_{n+1}(k_{d,\lambda} R)} \left(\left(\frac{1}{\pi} \int_0^{2\pi} G_0 \cos(n\theta) d\theta \right) \cos(n\theta) + \left(\frac{1}{\pi} \int_0^{2\pi} G_0 \sin(n\theta) d\theta \right) \sin(n\theta) \right) \tag{29}$$

If G_0 is constant at the reactor outer wall, then

$$G_\lambda =$$
$$\begin{cases} \frac{4 I_0(k_{d,\lambda} r) \left(\frac{1}{2\pi} \int_0^{\pi} G_0 d\theta \right)}{I_0(k_{d,\lambda} R) + \frac{2}{3\xi_\lambda} I_1(k_\lambda R)} + \sum_{n=1}^{+\infty} \frac{4 I_n(k_{d,\lambda} r)}{I_n(k_{d,\lambda} R) + \frac{2}{3\xi_\lambda} I_{n+1}(k_\lambda R)} \left(\left(\frac{1}{\pi} \int_0^{\pi} G_0 \cos(n\theta) d\theta \right) \cos(n\theta) + \left(\frac{1}{\pi} \int_0^{\pi} G_0 \sin(n\theta) d\theta \right) \sin(n\theta) \right), & if\ \theta \in [0;\pi] \\ \frac{4 I_0(k_{d,\lambda} r) \left(\frac{1}{2\pi} \int_\pi^{2\pi} G_0 d\theta \right)}{I_0(k_{d,\lambda} R) + \frac{2}{3\xi_\lambda} I_1(k_\lambda R)} + \sum_{n=1}^{+\infty} \frac{4 I_n(k_{d,\lambda} r)}{I_n(k_{d,\lambda} R) + \frac{2}{3\xi_\lambda} I_{n+1}(k_{d,\lambda} R)} \left(\left(\frac{1}{\pi} \int_\pi^{2\pi} G_0 \cos(n\theta) d\theta \right) \cos(n\theta) + \left(\frac{1}{\pi} \int_\pi^{2\pi} G_0 \sin(n\theta) d\theta \right) \sin(n\theta) \right), & if\ \theta \in [\pi;2\pi] \end{cases}$$
$$\tag{30}$$

2. 2 Cases of tubular and CPC photoreactors at a solar scale

A CPC reactor is a tubular reactor that receives radiation not only on its side exposed to the sun but also on its part hidden from the sun thanks to its two involutes, as depicted in Figure 1.
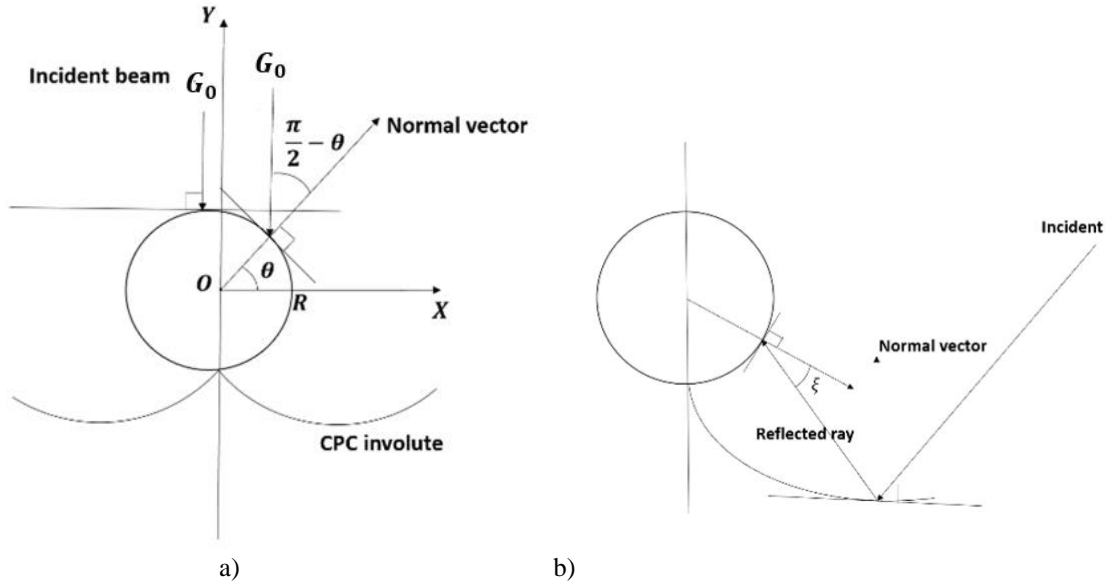
Figure 1. Boundary representation of radiation entrance with Lambert's cosine law on a CPC reactor. a) Incident beam arriving parallelly to the reactor axis, b) Ray-tracing technique simulation on CPC reactor, ξ is the angle between the reflected ray and the normal at a defined point on the lower side of the reactor tube.

In the case of CPC photocatalytic reactors, the integration constants Eq. (21) were determined using Marshak's boundary conditions with respect to the radial coordinate, assuming a collimated constant incident radiation arriving parallel to the reactor axis according to Figure 1 a). To achieve this, the light distribution at the upper and lower sides of the reactor tube ($f(\theta, G_0)$) as defined in Eq. (31) should be determined by using the ray-tracing technique [26] and then expanded into Fourier transform series.

$$f(\theta, G_0) = \begin{cases} f_1(\theta)G_0, & if \ \theta \in [0; \pi] \\ f_2(\theta)G_0, & if \ \theta \in [\pi; 2\pi] \end{cases} \tag{31}$$

where $f_1(\theta)$ and $f_2(\theta)$ are the fractions of light distribution at the upper and lower side of the reactor respectively and G_0 is the incident light intensity.

Considering Lambert's cosine law (irradiance) or fluence rate at the boundary, for the upper and lower-hemicylindrical reactor tubes and Marshak's boundary conditions, the specific intensity of the radiation is defined as follows:

$$G_\lambda = \frac{4I_0(k_{d,\lambda}r)\left(\frac{1}{2\pi}\int_0^{2\pi} G_0 d\theta\right)}{I_0(k_{d,\lambda}R)+\frac{2}{3\xi_\lambda}I_1(k_{d,\lambda}R)} + \sum_{n=1}^{+\infty} \frac{4I_n(k_{d,\lambda}r)}{I_n(k_{d,\lambda}R)+\frac{2}{3\xi_\lambda}I_{n+1}(k_{d,\lambda}R)}\left(\left(\frac{1}{\pi}\int_0^{2\pi} f\cos(n\theta)\,d\theta\right)\cos(n\theta) + \left(\frac{1}{\pi}\int_0^{2\pi} f\sin(n\theta)\,d\theta\right)\sin(n\theta)\right) \tag{32}$$

When Considering Lambert's cosine law (irradiance), $f_1(\theta)$ is defined as $sin(\theta)$ (Fig 1 a). For a tubular reactor at a solar scale with the same assumption as with the CPC reactor, since it does not receive radiation on its side hidden from the sun, the specific intensity of the radiation is defined by taking $f_2(\theta)$ equal to zero in Eqs. (31-32).

The optical thickness (τ) and the apparent optical thickness (τ_{App1}) in Eqs. (33-35) defined with the P1 approximation approach [28] were used in this work for optimization purposes.

$$\tau = (\sigma^* + \kappa^*)c_{cat}2R \qquad (33)$$

$$\tau_{App1} = \tau\sqrt{3\left(1 - \omega_{\lambda,mod}^2\right)} \qquad (34)$$

$$\omega_{\lambda,mod} = \sqrt{\omega_\lambda\left(1 + \frac{g_\lambda}{3} - \frac{g_\lambda}{3}\omega_\lambda\right)} \qquad (35)$$

3. Results and analysis

The model was applied to a heterogeneous photocatalytic solar CPC reactor based on TiO$_2$-P25, with the CPC reactor characteristics taken from the literature [26]. The incident radiation was assumed to be collimated and parallel to the reactor axis, and Lambert's cosine law was considered when applying the boundary conditions (Figure 1). The fraction of light intensity at the reactor wall used in this work, as shown in Figure 2, was reported in the literature [26].

**Table 1.** Parameters of the CPC reactor

Tube radius: R (m)	Varying
The CPC half-acceptance angle	56°
The solar UV radiation flux: I$_0$ (W/m^2)	30
The specific mass absorption κ (m^2/kg)	174.75
The scattering coefficient σ(m^2/kg)	1295.75
The specific mass absorption of a given contaminant: κ_c	Considered here equal to zero
The catalyst load: C_{cat}(g/l)	Starting from zero g/l
Asymmetry factor: g	0.53
The scattering albedo ω: $\frac{\sigma}{\sigma+\kappa+\kappa_c}$	0.88
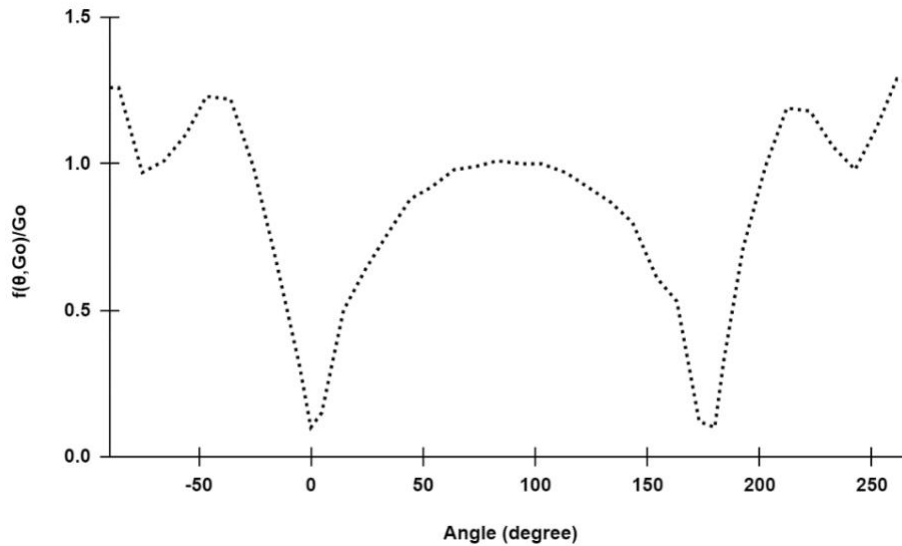
**Figure 2.** Fraction of light intensity at the reactor wall [26].

3. 1 Absorption behavior inside the CPC reactor

Figure 3 shows the *LVRPA* profile at different catalyst loadings where it is observed a decrease of the *LVRPA* from the reactor wall to its center for each value of catalyst loading. It is also observed that the *LVRPA* increases with catalyst loading especially at the zones near the reactor wall while it decreases at the zones close to the reactor center. This figure displays an increase of the *LVRPA* from $\theta = 0$ to $\theta = \frac{\pi}{2}$ since the incident radiation varies as the sine function of the angular variable according to Lambert's cosine law [15], [25-27] and as depicted in Figure 1a.

a) Ccat = 0.1 g/L

b) Ccat = 0.3 g/L

c) Ccat = 0.5 g/L

d) Ccat = 0.7 g/L
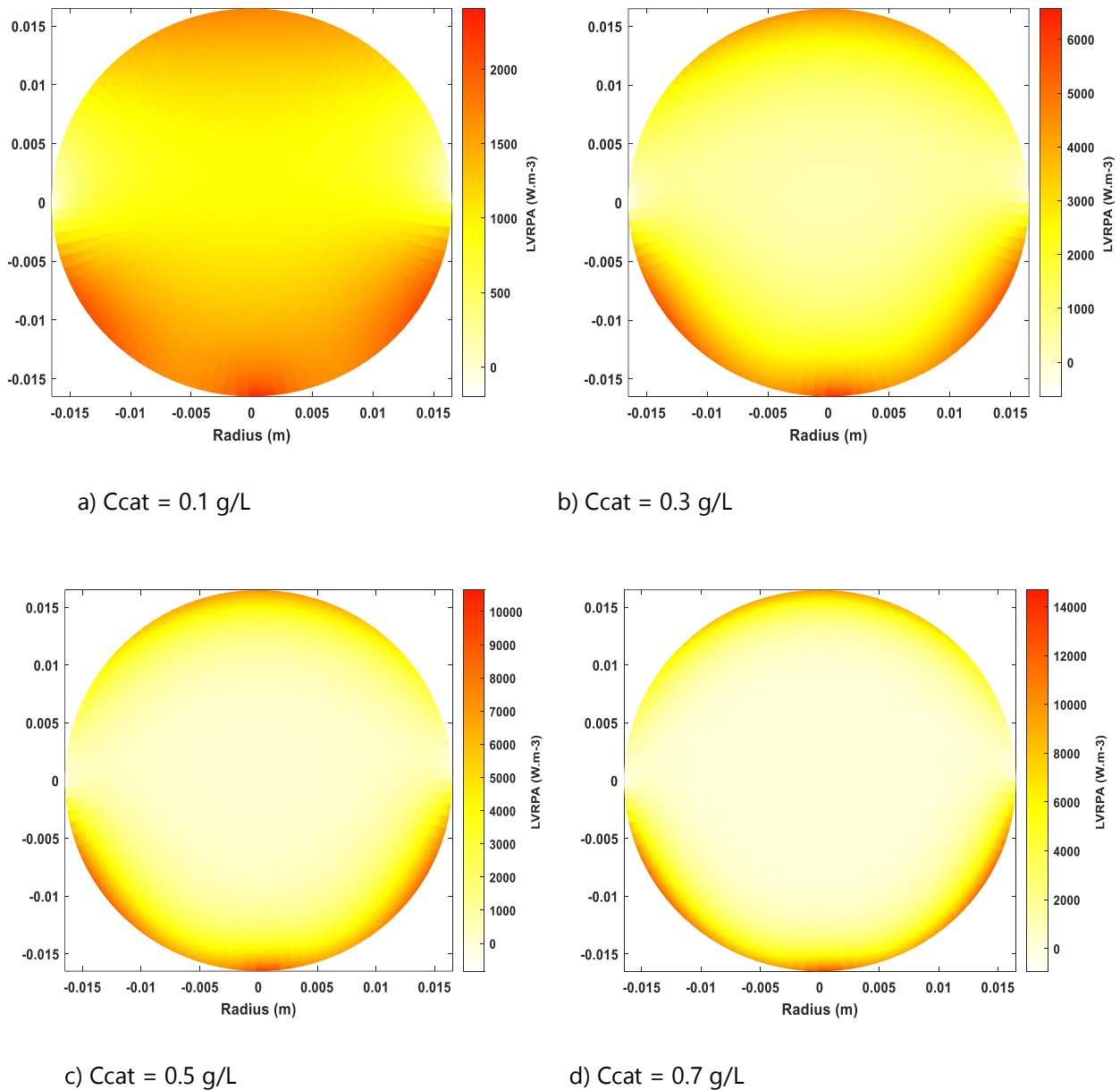
Figure 3. The *LVRPA* profile for different catalyst loadings on a transversal section of the CPC reactor of radius 1.65 cm.

For very high values of catalyst loading (greater than 0.5 g/L), photon absorption becomes very competitive due to the saturation of the catalyst particles in the zone close to the reactor wall, which impedes photon penetration to the inner part of the reactor. A good uniformization of photon absorption was observed for a small amount of catalyst and was found to decrease with the increase in catalyst loading. These observations agree with the literature [3], [25].
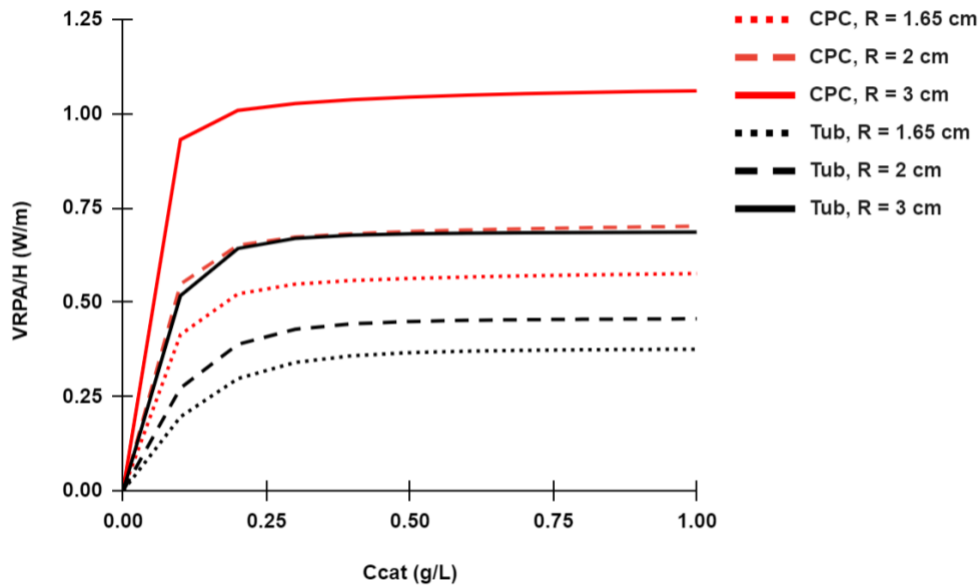
Figure 4. The $VRPA/H$ as a function of catalyst loading, red and black lines represent the $VRPA/H$ on the CPC and tubular reactors respectively. Straight, interrupted and dotted lines represent the $VRPA/H$ for reactor radius equal to 3, 2, and 1.65 cm respectively.

For the determination of the optimum catalyst loading, the $VRPA/H$ was simulated, and Figure 4 shows how it varies as a function of catalyst loading for different values of reactor radius on CPC and tubular reactors. The red and black lines represent the $VRPA/H$ on the CPC and tubular reactors respectively, where straight, interrupted and dotted lines represent the $VRPA/H$ for reactor radius equal to 3, 2, and 1.65 cm respectively. This figure displays for both reactors an exponential increase of the $VRPA/H$ with catalyst loading until a fixed value from where no significant increase is observed. Therefore, working above this value could lead to catalyst waste which is not beneficial for the photocatalytic process from an economic point of view. It was found that the $VRPA/H$ increased with the reactor radius, this could be explained by the fact that increasing the reactor radius enhances the probability of photon interaction with catalyst particles. Nevertheless, an excessive increase in reactor radius could disfavor the photon absorption inside the reactor since the photon pathway to the inner zones of the reactor could increase significantly and photons will hardly reach the reactor's deeper zones. A reactor radius in the range of 1.25-2.5 cm was found adequate for these types of reactors [31], [32]. The graphic in Figure 4 shows that the optimum catalyst loading decreases with the increase of the reactor radius which is in good agreement with the literature [33]. At 0.3 g/L of catalyst loading, the $VRPA/H$ was found in this work about 0.59 W/m and 1.01 W/m with the SFM-2D-HG [25]. The discrepancy stands due to the fact that the light distribution at the lower side of the CPC reactor was not used accurately when implementing the SFM-2D-HG [25]. It is worth mentioning that SFM-2D-HG and SFM-2D-DR stand for the six-flux model in two dimensions with Heyney-Greenstein and diffuse reflectance phase functions respectively. The $VRPA/H$ on CPC reactor was 51 % higher than that on the tubular reactor with irradiance

which agrees with the literature when using SFM-2D-HG [25] which is evident since the tubular reactor does not receive radiation on its side hidden from the sun while the CPC reactor does receive. It was also found that the optimum catalyst loading for CPC reactors is 50 % less than that with tubular reactors, which shows how efficient are CPC reactors compared to tubular reactors. This result is not far from that found in the literature [24]. The use of the irradiance in this work was justified by the fact that it was found that using the irradiance at the boundary conditions is better than using the fluence rate [15]. It is then recommended to use irradiance at the boundary conditions when employing the P1 approximation as is the case with the SFM.

Table 2. Optimum catalyst loading (C_{op} (g/L)), optical thickness (τ_{op}), apparent optical thickness ($\tau_{App1,op}$), and the $VRPA/H$ ($VRPA/H_{op}$) in W/m for different reactor radius on the CPC and tubular reactors.

	Tub	reactor			CPC	reactor		
R (cm)	C_{op}	τ_{op}	$\tau_{App1,op}$	$VRPA/H_{op}$	C_{op}	τ_{op}	$\tau_{App1,op}$	$VRPA/H_{op}$
1.65	0.545	26.48	14.6	0.368	0.364	17.65	9.73	0.555
2	0.45	26.47	14.59	0.446	0.3	17.65	9.73	0.673
3	0.3	26.47	14.59	0.67	0.2	17.65	9.73	1.0091

The optimum catalyst loading is found in Table 2 for three different reactor radii, as well as the optimum optical thickness, apparent optical thickness and $VRPA/H$ on the CPC and tubular reactors. For both reactors, C_{op} was found to decrease with the increase of the reactor radius while τ_{op} and $\tau_{App1,op}$ remain insensitive with the change in the reactor radius. Therefore τ_{op} and $\tau_{App1,op}$ remove the dependence of the optimum catalyst loading on reactor radius and stand as more reliable optimization parameters than C_{op}.

Table 3. Optimum catalyst loading, optical thickness, apparent optical thickness, and $VRPA/H$ for different catalyst albedo (R = 1.65 cm, κ = 174.75 m²/kg) on CPC and tubular reactors.

	Tub	reactor			CPC	reactor		
ω	C_{op}	τ_{op}	$\tau_{App1,op}$	$VRPA/H_{op}$	C_{op}	τ_{op}	$\tau_{App1,op}$	$VRPA/H_{op}$
0.75	0.78	17.99	14.51	0.477	0.523	12.064	9.73	0.709
0.8	0.71	20.47	14.69	0.444	0.47	13.55	9.73	0.662
0.85	0.61	23.45	14.5	0.402	0.401	15.76	9.75	0.604
0.95	0.36	41.52	14.67	0.266	0.24	27.68	9.78	0.407

Apart from removing the dependence of the optimum catalyst loading on the reactor radius, $\tau_{App1,op}$ seems to be almost insensitive with the change in the catalyst albedo which is not the case with τ_{op} which fluctuated significantly as shown in Table 3. Table 3 displays the optimum optical thickness and apparent optical thickness for different catalyst albedos and scattering coefficients with a fixed specific mass absorption coefficient (κ = 174.75 m²/kg) for both types of reactors. As a result, the perceived optical thickness is a more reliable dimensionless optimization parameter than optical thickness. The recommended apparent optical thickness that leads to the optimum operating conditions is around 9.73 and 14.6 for CPC and tubular reactors respectively. This parameter formulated with the P1 approximation approach was newly introduced by Clovis Nchikou on flat plate photocatalytic reactors and was found around 4.87 [28]. By using Eq. (33-35), the couples (R, C_{op}) that optimize the radiation absorption inside CPC and tubular reactors can be found. The $VRPA/H_{op}$ seems to decrease with the increase in scattering albedo which is obvious since this implies the decrease in the capacity of absorption of the catalyst.

4. Perspectives

Future work will formulate the *LVRPA* in 3D on CPC and tubular reactors with the P1 approximation approach (P1-3D).

Conclusion

The *LVRPA* was derived in polar coordinates with the P1 approximation approach for cylindrical photocatalytic reactors with the incident radiation supposed to be constant along the reactor height, and then the cases involving CPC and tubular reactors were addressed. The results found when simulating the model were close to those in the literature. A dimensional parameter τ_{App1} was introduced and was found to be reliable for optimization purposes. The information presented here is crucial because it avoids the need for statistical analysis of experimental designs and the employment of robust models to solve the RTE, both of which involve major time and financial investment. This could also be useful in creating a rate equation to characterize the kinetics of photocatalytic degradation of diverse substances.

Competing Interests
The author has no conflict of interest to declare.

Funding
The author received no specific funding for this work.

References

[1] He, C., Clifton, O., Felker-Quinn, E., Fulgham, S. R., Juncosa Calahorrano, J. F., Lombardozzi, D., Purser, G., Riches, M., Schwantes, R., Tang, W., Poulter, B., & Steiner, A. L. (2021). Interactions between Air Pollution and Terrestrial Ecosystems: Perspectives on Challenges and Future Directions. Bulletin of the American Meteorological Society, 102(3), E525– E538. https://doi.org/10.1175/BAMS-D-20-0066.1

[2] Nair, A. K., & JagadeeshBabu, P. E. (2017). Ag-TiO2 nanosheet embedded photocatalytic membrane for solar water treatment. Journal of Environmental Chemical Engineering, 5(4), 4128–4133. https://doi.org/10.1016/j.jece.2017.07.046

[3] Diaz-Angulo, J., Lara-Ramos, J., Mueses, M., Hernández-Ramírez, A., Li Puma, G., & Machuca-Martínez, F. (2020). Enhancement of the oxidative removal of diclofenac and of the TiO2 rate of photon absorption in dye-sensitized solar pilot scale CPC photocatalytic reactors. *Chemical Engineering Journal*, *381*, 122520. https://doi.org/10.1016/j.cej.2019.122520

[4] Rizzo, L., Malato, S., Antakyali, D., Beretsou, V. G., Đolić, M. B., Gernjak, W., Heath, E., Ivancev-Tumbas, I., Karaolia, P., Lado Ribeiro, A. R., Mascolo, G., McArdell, C. S., Schaar, H., Silva, A. M. T., & Fatta-Kassinos, D. (2019). Consolidated vs new advanced treatment methods for the removal of contaminants of emerging concern from urban wastewater. *Science of The Total Environment*, *655*, 986–1008. https://doi.org/10.1016/j.scitotenv.2018.11.265

[5] Vaya, D., & Surolia, P. K. (2020). Semiconductor based photocatalytic degradation of pesticides: An overview. *Environmental Technology & Innovation*, *20*, 101128. https://doi.org/10.1016/j.eti.2020.101128

[6] Wang, D., Mueses, M. A., Márquez, J. A. C., Machuca-Martínez, F., Grčić, I., Peralta Muniz Moreira, R., & Li Puma, G. (2021). Engineering and modeling perspectives on photocatalytic reactors for water treatment. *Water Research*, *202*, 117421. https://doi.org/10.1016/j.watres.2021.117421

[7] Ochoa-Gutiérrez, K. S., Tabares-Aguilar, E., Mueses, M. Á., Machuca-Martínez, F., & Li Puma, G. (2018). A Novel Prototype Offset Multi Tubular Photoreactor (OMTP) for solar photocatalytic degradation of water contaminants. *Chemical Engineering Journal*, *341*, 628–638. https://doi.org/10.1016/j.cej.2018.02.068

[8] Colina-Márquez, J., Machuca-Martínez, F., & Li Puma, G. (2015). Modeling the Photocatalytic Mineralization in Water of Commercial Formulation of Estrogens 17-β Estradiol (E2) and Nomegestrol Acetate in Contraceptive Pills in a Solar Powered Compound Parabolic Collector. *Molecules*, *20*(7), 13354–13373. https://doi.org/10.3390/molecules200713354

[9] Illi, E., Bouanani, F. E., Park, K.-H., Ayoub, F., & Alouini, M.-S. (2019). An Improved Accurate Solver for the Time-Dependent RTE in Underwater Optical Wireless Communications. *IEEE Access*, *7*, 96478–96494. https://doi.org/10.1109/ACCESS.2019.2929122

[10] Fujii, H., Terabayashi, I., Aoki, T., Inoue, Y., Na, H., Kobayashi, K., & Watanabe, M. (2022). Numerical Study of Near-Infrared Light Propagation in Aqueous Alumina Suspensions Using the Steady-State Radiative Transfer Equation and Dependent Scattering Theory. *Applied Sciences*, *12*(3), 1190. https://doi.org/10.3390/app12031190

[11] Ghafoori, S., Nasirian, M., Al-Jamal, R., Mallouh, F. A., & Mehrvar, M. (2020). Statistical parameter optimization and modeling of photodegradation of methyl orange using a composite photocatalyst prepared by thermal synthesis. *Environmental Science and Pollution Research*, *27*(36), 45650–45660. https://doi.org/10.1007/s11356-020-10301-5

[12] Howell, J. R., Mengüç, M. P., Daun, K. J., & Siegel, R. (2021). *Thermal radiation heat transfer* (Seventh edition). CRC Press */Taylor & Francis Group, Boca Raton, FL (USA)*, 53-93.

[13] Acosta-Herazo, R., Cañaveral-Velásquez, B., Pérez-Giraldo, K., Mueses, M. A., Pinzón-Cárdenas, M. H., & Machuca-Martínez, F. (2020). A MATLAB-Based Application for Modeling and Simulation of Solar Slurry Photocatalytic Reactors for Environmental Applications. *Water*, *12*(8), 2196. https://doi.org/10.3390/w12082196

[14] Moreno-SanSegundo, J., Casado, C., & Marugán, J. (2020). Enhanced numerical simulation of photocatalytic reactors with an improved solver for the radiative transfer equation. *Chemical Engineering Journal*, *388*, 124183. https://doi.org/10.1016/j.cej.2020.124183

[15] Peralta Muniz Moreira, R., & Li Puma, G. (2021). Multiphysics Computational Fluid-Dynamics (CFD) Modeling of Annular Photocatalytic Reactors by the Discrete Ordinates Method (DOM) and the Six-Flux Model (SFM) and Evaluation of the Contaminant Intrinsic Kinetics Constants. *Catalysis Today*, *361*, 77–84. https://doi.org/10.1016/j.cattod.2020.01.012

[16] Arancibia-Bulnes, C. A., Jiménez, A. E., & Estrada, C. A. (2009). Development and Modeling of Solar Photocatalytic Reactors. In Advances in Chemical Engineering (Vol. 36, pp. 185– 227). Elsevier. https://doi.org/10.1016/S0065-2377(09)00406-2

[17] Cuevas, S. A., Arancibia-Bulnes, C. A., & Serrano, B. (2007). Radiation Field in an Annular Photocatalytic Reactor by the P1 Approximation. *International Journal of Chemical Reactor Engineering*, *5*(1). https://doi.org/10.2202/1542-6580.1589

[18] Akdemir, O., Lagendijk, A., & Vos, W. L. (2022). Breakdown of light transport models in photonic scattering slabs with strong absorption and anisotropy. *Physical Review A*, *105*(3), 033517. https://doi.org/10.1103/PhysRevA.105.033517

[19] Christenson, J. G., Austin, R. A., & Phillips, R. J. (2018). Comparison of approximate solutions to the phonon Boltzmann transport equation with the relaxation time approximation: Spherical harmonics expansions and the discrete ordinates method. *Journal of Applied Physics*, *123*(17), 174304. https://doi.org/10.1063/1.5022182

[20] Harel, R., Burov, S., & Heizler, S. I. (2021). Asymptotic P_N Approximation in Radiative Transfer Problems. *Journal of Computational and Theoretical Transport*, *50*(5), 390–406. https://doi.org/10.1080/23324309.2020.1845738

[21] Cuevas, S. A., & Arancibia-Bulnes, C. A. (n.d.). *Modeling UV radiation absorption in a flat-plate photocatalytic reactor*.

[22] Abdel-Maksoud, Y., Imam, E., & Ramadan, A. (2016). TiO2 Solar Photocatalytic Reactor Systems: Selection of Reactor Design for Scale-up and Commercialization—Analytical Review. *Catalysts*, *6*(9), 138. https://doi.org/10.3390/catal6090138

[23] Muscetta, M., Ganguly, P., & Clarizia, L. (2024). Solar-powered photocatalysis in water purification: Applications and commercialization challenges. *Journal of Environmental Chemical Engineering*, *12*(3), 113073. https://doi.org/10.1016/j.jece.2024.113073

[24] Colina-Márquez, J., Machuca-Martínez, F., & Puma, G. L. (2010). Radiation Absorption and Optimization of Solar Photocatalytic Reactors for Environmental Applications. *Environmental Science & Technology*, *44*(13), 5112–5120. https://doi.org/10.1021/es100130h

[25] Nchikou, C., Loredo-Medrano, J. Á., Hernández-Ramírez, A., Colina-Marquez, J. Á., & Mueses, M. Á. (2021). Estimation of the radiation field for CPC photocatalytic reactors using a novel six-flux model in two dimensions (SFM-2D). *Journal of Environmental Chemical Engineering*, *9*(6), 106392. https://doi.org/10.1016/j.jece.2021.106392

[26] Ren, Y., Zhao, L., Jing, D., & Guo, L. (2016). Investigation and modeling of CPC-based tubular photocatalytic reactor for scaled-up hydrogen production. *International Journal of Hydrogen Energy*, *41*(36), 16019–16031. https://doi.org/10.1016/j.ijhydene.2016.04.225

[27] Reifsnyder, W. E. (1967). Radiation geometry in the measurement and interpretation of radiation balance. *Agricultural Meteorology*, *4*(4), 255–265. https://doi.org/10.1016/0002-1571(67)90026-X

[28] Nchikou, C. (2024). Estimation and Optimization of the Radiant Field in Flat Plate Heterogeneous Photoreactors with the P1-approximation of the Radiative Transfer Equation (RTE). *Journal of the Turkish Chemical Society Section B: Chemical Engineering*, 87–104. https://doi.org/10.58692/jotcsb.1450662

[29] Tourasse, G., & Dumortier, D. (2014). Development of a System Measuring the Solar Radiation Spectrum in 5 Planes for Daylight and PV Applications. *Energy Procedia*, *57*, 1110–1119. https://doi.org/10.1016/j.egypro.2014.10.071

[30] Marshak, R. E. (1947). Theory of the Slowing Down of Neutrons by Elastic Collision with Atomic Nuclei. Reviews of Modern Physics, 19(3), 185–238. https://doi.org/10.1103/RevModPhys.19.185

[31] Dillert, R., Cassano, A. E., Goslich, R., & Bahnemann, D. (1999). Large scale studies in solar catalytic wastewater treatment. *Catalysis Today*, *54*(2–3), 267–282. https://doi.org/10.1016/S0920-5861(99)00188-1

[32] Guillard, C., Disdier, J., Herrmann, J.-M., Lehaut, C., Chopin, T., Malato, S., & Blanco, J. (1999). Comparison of various titania samples of industrial origin in the solar photocatalytic detoxification of water containing 4-chlorophenol. *Catalysis Today*, *54*(2–3), 217–228. https://doi.org/10.1016/S0920-5861(99)00184-4

[33] Fernández-Ibáñez, P., Malato, S., & De Las Nieves, F. J. (1999). Relationship between TiO2 particle size and reactor diameter in solar photoreactors efficiency. *Catalysis Today*, *54*(2–3), 195–204. https://doi.org/10.1016/S0920-5861(99)00182-0